Eur. Phys. J. B **78**, 173–186 (2010)
DOI: 10.1140/epjb/e2010-10333-4

THE EUROPEAN PHYSICAL JOURNAL B

Regular Article

Bistability and explosive transients in surface reactions: the role of fluctuations and spatial correlations

Y. De Decker[1,a] and F. Baras[2]

[1] Center for Nonlinear Phenomena and Complex Systems, Université Libre de Bruxelles (U.L.B.), Campus Plaine, C.P. 231. 1050 Brussels, Belgium
[2] Laboratoire interdisciplinaire Carnot de Bourgogne, UMR 5209 CNRS-Université de Bourgogne, 21078 Dijon Cedex, France

Received 26 April 2010 / Received in final form 13 September 2010
Published online 12 November 2010 – © EDP Sciences, Società Italiana di Fisica, Springer-Verlag 2010

Abstract. We study the dynamics of a class of catalytic surface reactions in which an adsorbed molecule undergoes dissociation giving oxygen, which then rapidly reacts with H adatoms to give water. The reaction-diffusion equations predict bistability and explosive transients similar to those observed in several low-pressure experiments. Kinetic Monte Carlo simulations reveal however that the dynamics can be strongly affected by spontaneous, inhomogeneous fluctuations of composition on the surface. In particular, bifurcation points can be displaced and the explosive character of the transients can be lost, depending on a subtle balance between the rate of reaction and the mobility of the decomposing species. These effects can be quantified on the basis of a stochastic formulation of the dynamics taking into account spatial correlations. This approach allows to better delimit the applicability of the traditional reaction-diffusion modelling in the case of reactions such as the reduction of NO_x or SO_x species on catalytic surfaces.

1 Introduction

Solid-gas heterogeneous catalysis forms a prototypical example of reactive systems maintained far from equilibrium: reactants are typically continuously incorporated in a reactor, where they undergo chemical transformations on the surface of a solid support, while products of this reaction are rapidly pumped away. It is thus not surprising that a rich variety of complex phenomena have been observed for surface reactions in idealized and controlled out-of-equilibrium conditions (see for example [1]). These phenomena are often accompanied by a spatial reorganization of adsorbed molecules and/or a reconstruction of the surface; the scale of these structures can range from tens of micrometers down to only a few nanometers.

The existence of such small structures is not surprising per se. Surfaces are low-dimensional supports that constrain the environment of the adsorbed species both for the reactive and the transport processes. Because of such geometrical restrictions, the inhomogeneous fluctuations of surface composition or structure arising spontaneously are not easily washed out and can, in appropriate circumstances, amplify and dictate the overall dynamics [2–8]. From the point of view of modelling, the existence of these fluctuations requires the development of theoretical approaches which go beyond the traditional mass-action law and reaction-diffusion equations based on the *mean field* (MF) approximation [9–11] [1].

Most theoretical studies concerning the effects of inhomogeneous fluctuations were restricted to the modification of the stationary properties and oscillatory behaviors of monomer-monomer or monomer-dimer surface reactions. In this paper, we study a prototypical class of surface reactions where one of the reactants must undergo dissociation before the final products can be formed – a situation found in fact in a majority of heterogeneous catalytic reactions like for instance the hydrogenation of CO, NO_x and SO_x species. The decomposition of such molecules thus involves different adjacent surface sites. This aspect enhances the intrinsic nonlinearity of the reaction which may lead to unexpected behaviors.

As will be shown, this class of systems is characterized by bistability and reaction-induced isothermal explosive transitions. This particular behavior consists in a long and transient induction period followed by a sudden transition leading to the final steady state, and has been observed in many instances of surface reactions. The main question we will address here is whether reaction-diffusion equations adequately describe the dynamics of surface reactions in this case. Our strategy will be to compare the results of

[a] e-mail: ydedecke@ulb.ac.be

[1] By mean field we here refer to the approximation where all particles are statistically uncorrelated. This level of description is also referred to as the "single site" approximation in the case of lattice systems.

stochastic, kinetic Monte Carlo (KMC) simulations with the MF predictions in order to detect the situations for which the traditional kinetic description "breaks down". The connection between these two levels of description can be made on the basis of the master equation (ME) associated with the microscopic mechanism of the reaction. When necessary, amended kinetic laws can be derived on the basis of the "exact" dynamics provided by this ME, emphasizing the limits of the MF approach in describing the simulations. Strong deviations between MF results and KMC simulations have been detected in this way for non-equilibrium surface reactions in which adsorbates are supposed to remain immobile [12–14]. In the present study, we will investigate in detail the role played by the surface transport of adsorbates. This will allow us to quantify the conditions for which the mobility is strong enough to recover the mass-action laws, both in simulations and in the ME-based approach.

In the following section we introduce the Langmuir-Hinshelwood model used in our study. The stationary and transient properties of the model predicted by the MF description will be presented. Despite its simplicity, the model qualitatively reproduces several phenomena that have been observed in low-pressure experiments for this type of reactive systems. Section 3 is devoted to the description of the stochastic approach. Starting from the reactive dynamics as described by the ME, we derive the traditional MF evolution equations together with amended kinetic equations taking into account the existence of spatial correlations between pairs of adsorbed particles. The algorithm of corresponding simulations is also described. In Section 4, we show that the stationary states and the explosions generated by the simulations can be strongly affected by fluctuations, leading in some circumstances to a loss of bistability and explosive behavior at the macroscopic scale. The diffusion of particles is in this view essential for the synchronization of different regions of the surface; we show in particular how this can be deduced from the amended evolution equations previously derived. Finally, we discuss in the last section the relevance of the results presented here and point out some future developments.

2 A Simple Langmuir-Hinshelwood model

Heterogeneous catalytic reactions typically involve adsorption of molecules from the gas phase onto a solid substrate (typically, a transition metal), and subsequent reactions of the adsorbed species to form the products. As was mentioned earlier, most investigations on the limits of the traditional kinetic laws focused on systems where the different adsorbates simply react together when they are sufficiently close to each other. In real-world systems one or several of the reactants first undergo a decomposition into some intermediates which then combine to give the final products. This is for example the case for the reduction by H_2 of NO_x molecules on platinum, a system which actually formed the basis of this model [15], but also other oxygen-containing species such as carbon monoxide or sulfur oxides. This class of hydrogenation reactions will form the basis of the qualitative model that will be studied here. Supposing that the oxygen-rich species, which we will denote X, adsorbs molecularly we get

$$\mathrm{X}(g) + * \underset{k_{-1}}{\overset{k_1}{\rightleftharpoons}} \mathrm{X}(ads) \tag{1}$$

$$\mathrm{H_2}(g) + 2* \underset{k_{-2}}{\overset{k_2}{\rightleftharpoons}} 2\mathrm{H}(ads) \tag{2}$$

where $*$ is an empty surface site, and (g) and (ads) represent gas-phase and adsorbed particles, respectively. H_2 is well known to dissociate upon adsorption on most transition metals and thus acts as a "dimer" in the reaction scheme.

The oxygen-containing molecule typically decomposes then to give an adsorbed oxygen atom and an intermediate product, say X′. This process requires the presence of an adjacent empty surface site:

$$\mathrm{X}(ads) + * \underset{k'_d}{\overset{k_d}{\rightleftharpoons}} \mathrm{X}'(ads) + \mathrm{O}(ads).$$

The oxygen formed in this way can subsequently react with adsorbed hydrogen atoms to give water which usually readily desorbs from the metallic surface, leaving three free sites

$$\mathrm{O}(ads) + 2\mathrm{H}(ads) \overset{k_R}{\rightarrow} 3* + \mathrm{H_2O}(g).$$

We will consider the decomposition of X to be the rate limiting step of the overall hydrogenation process: in other words the intermediate products are quickly removed by reaction and/or desorption. The intermediate steps can then be lumped into a single decomposition-hydrogenation process reading

$$\mathrm{X}(ads) + * + 2\,\mathrm{H}(ads) \overset{k_3}{\rightarrow} 4* + \mathrm{X}'(g) + \mathrm{H_2O}(g). \tag{3}$$

In this view, the kinetic constant k_3 is a combination of the rate constants of the different sub-steps.

As can be seen in equation (3), the simple model we present here is characterized by a strongly autocatalytic empty site production step which arises from the combination of the empty site requirement for the decomposition of X and a rapid reactive step that tends to empty the surface. Analyzing previously developed models for surface explosions, it appears that this site requirement is a common feature shared by most systems of the class we analyze here. This is the case for example for the NO+CO reaction on Pt, for which Lesley and Schmidt proposed that the empty site requirement of the NO decomposition process was central to their observations [16]. Detailed mean-field and atomistic modelling further supported the idea that empty site requirement was the main driving force behind the observed explosive and oscillatory behaviors in that case [17–19]. A similar autocatalytic step can also be found for example, in mean-field as well as atomistic models for the NO+H_2 [20–24] or NO+NH_3 [25,26] reactions on Pt or the N_2O+H_2 reaction on Ir [27]. A vacancy-induced mechanism was also invoked for the decomposition of acetate on Rh, Ni and Pd, although in that case the

regeneration of empty sites seems to be primarily due to desorption (and not a subsequent reaction) [28]. The simple effective mechanism (1)–(3) we derived here can thus be seen as a "backbone" description that summarizes the most important features of mainly previously developed models of surface explosions. It should be also emphasized that most of these models stipulate or reveal that the decomposition mainly occurs through a sort of "island" formation, i.e. that the decomposition mainly takes place at the boundary between densely covered and almost empty regions of the surface.

Mean field kinetics

In the MF approach, the chemical composition of surfaces is usually described through the coverages of the different species, which are defined as the fractions of active sites occupied by the corresponding adsorbate. This coverage can be defined globally (over the whole surface) as well as locally, by dividing the system into mesoscopic boxes centered around macroscopic coordinates $\mathbf{r}$. In most of the experiments performed in surface chemistry, the temperature and the partial pressures are maintained constant. The kinetics on the surface is thus entirely described by a set of reaction-diffusion equations for the above mentioned local coverages:

$$\frac{\partial}{\partial t}x(\mathbf{r},t) = k_1 p_{\mathrm{X}} s - k_{-1} x - k_3 x s h^2 + D_{\mathrm{X}}(1-h)\nabla^2 x + D_{\mathrm{X}} x \nabla^2 h \qquad (4)$$

$$\frac{\partial}{\partial t}h(\mathbf{r},t) = 2k_2 p_{\mathrm{H}_2} s^2 - 2k_{-2} h^2 - 2k_3 x s h^2 + D_{\mathrm{H}} h \nabla^2 x + D_{\mathrm{H}}(1-h)\nabla^2 h \qquad (5)$$

where x, h and s represent the different coverages in X, H and empty sites, respectively. D_{X} and D_{H} are the diffusion coefficients of the two reactants, and p_{X} and p_{H_2} are their partial pressure in the surrounding gas. Note that because the total number of site is conserved, we have $x+h+s=1$. This conservation reflects itself in the adsorption terms, which are not constant but "saturate", and in the diffusion terms that are as a consequence nonlinear (see Appendix A for details on the derivation of these terms from the local chemical potentials). It should be emphasized that using traditional Fickian diffusion leads to a nonconservative diffusion process since the sum of the diffusion fluxes is nonzero. Note also that for reasons of clarity we do not write explicitly the spatiotemporal dependance in the right-hand side and that we consider a normalized space for which the diffusion coefficients are expressed in s^{-1}.

The evolution equations (4)–(5) contain several reaction and diffusion parameters whose exact value depends on the nature of X and of the substrate on which the reaction takes place. As our goal here is to investigate the qualitative behavior of this class of systems, we may use rough estimates of these different parameters for our analysis. Hydrogen is for example known to desorb quite rapidly from most transition metals already at room temperature; accordingly, its diffusion is also quite rapid [29]. The desorption and diffusion rates of the other reactant depend on its exact nature, but will typically be much lower than that of hydrogen at any temperature. Concerning adsorption, $k_1\ p_X$ and $k_2\, p_{\mathrm{H}_2}$ can act as effectively adjustable parameters, since the pressures can be modified more or less at will in the types of systems studied here. The (lumped) decomposition-hydrogenation rate constant k_3 is more difficult to evaluate, even qualitatively. Relatively unstable species, such as nitrogen oxides, will tend to decompose at a nonnegligible rate at sufficiently high temperatures, while more stable species such as CO could keep a relatively low decomposition probability at any time. Given the scope of this study, k_3 should thus be seen as a *parameter* that is representative of the nature of the reactant X.

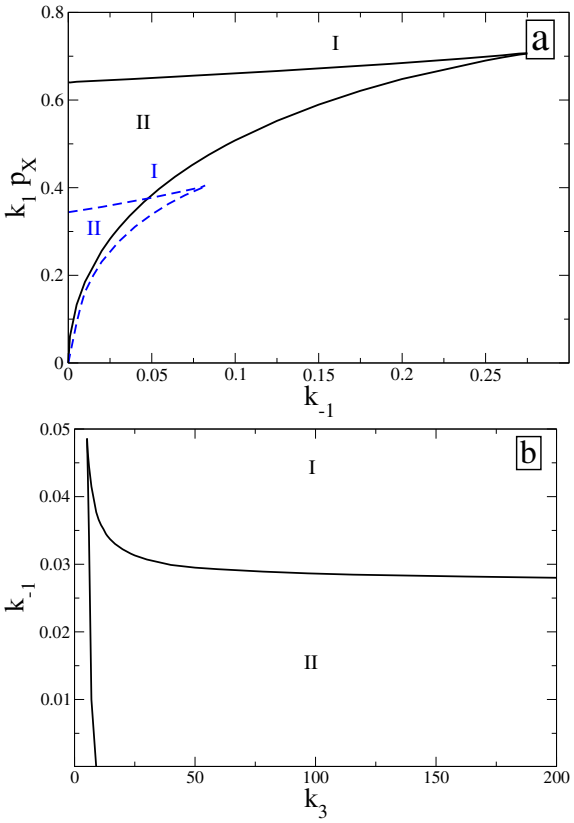

Fig. 1. (Color online) Two-parameter diagrams, plotting the boundaries between monostability (zones I) and bistability (zones II) for $k_2\, p_{\mathrm{H}_2} = 1\ \mathrm{s}^{-1}$ and $k_{-2} = 0.1\ \mathrm{s}^{-1}$. (a) Plots the critical X adsorption rate constant as a function of the X desorption rate constant, for $k_3 = 100\ \mathrm{s}^{-1}$ (plain black lines) and $k_3 = 10\ \mathrm{s}^{-1}$ (dashed blue lines). (b) Shows the critical k_{-1} as a function of k_3 for $k_1\, p_{\mathrm{X}} = 0.3\ \mathrm{s}^{-1}$.

The steady state properties of the model were investigated in the homogeneous limit using the AUTO-07p continuation package. The main conclusions are summarized in Figures 1 and 2, showing 2-parameters and 1-parameter bifurcation diagrams. Multistationarity, or more precisely bistability, can be found in a well defined region of the parametric space (Figs. 1a–1b). It is typically sandwiched

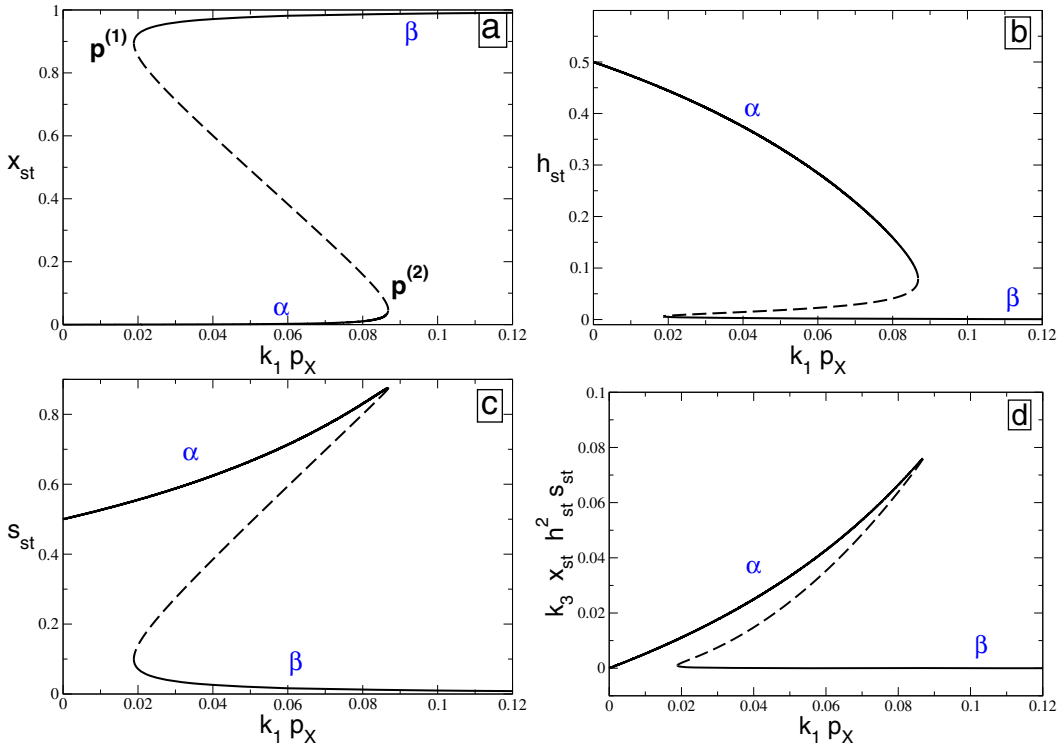

Fig. 2. (Color online) One-parameter state diagrams obtained with $k_{-1} = 0.001$ s^{-1}, $k_2\, p_{H_2} = k_{-2} = 0.1$ s^{-1} and $k_3 = 300$ s^{-1}. Stable states are denoted by plain curves and unstable ones with dashed lines. The figures plot respectively the stationary (a) coverage in X, (b) coverage in H, (c) fraction of empty sites and (d) reaction rate ($k_3\, x\, h^2\, s$). The αs and βs refer to the reactive and quasi-poisoned states (see text).

between two critical values of the effective adsorption rate constants (and hence of partial pressures) whose values themselves depend on the decomposition and desorption rates. The width of this zone decreases when increasing k_{-1} (the desorption rate constant of X) and increases with k_3. The hydrogen desorption rate constant k_{-2} has little to no effect, as long as it remains much larger than the X desorption rate constant, which is more than probably the case, as discussed earlier. In the zone of multistability, three states coexist (two stable states and one unstable state) which correspond to distinctly different surface compositions.

This is depicted for example in Figure 2, where the final X coverage, H coverage, fraction of empty sites and rate of water production are plotted as a function of the effective adsorption rate constant (all the other parameters being maintained constant). Starting from low $k_1\, p_X$, the surface lies in a state of low coverage (from here on referred to as the α state) where the reaction rate is relatively important (see Fig. 2d). On the other extreme, starting from high values, the model predicts a highly X-covered surface with very low reactivity, which will be referred to as the β state. For intermediate pressures, the two mentioned surface states can coexist and are separated by an unstable state of intermediate coverage and reactivity.

The very existence of a bistability is central in our study, because of the peculiar dynamics of systems starting close to a turning point, but slightly outside of the domain of existence of the neighboring state. The corresponding transients are known to be explosive, i.e. they are characterized by a long waiting period followed by an abrupt change in composition. The system we study here presents two turning points: one corresponds to a surface mostly covered by X, while the other one can be assimilated to a rather empty system. We will focus here on the behavior around the "upper" turning point (namely, in the vicinity of the β state) because explosive phenomena starting from highly covered surfaces have been observed in many instances of surface chemical reactions of the type we analyze here. For the NO+H_2 reaction, a rapid and transitory increase of the rate of water production has been observed during temperature-programmed reactions on single surfaces initially highly covered by nitrogen monoxide. This behavior was observed on several transition metals, including Pt [21–24], Rh, Pd, Ir and Ru [30]. Associated waves of reaction were also observed using microscopy techniques when starting from a NO-covered surface, e.g. for isolated Pt surfaces [31] as well as for Pt tips presenting different cristallographic orientations [15,32–36]. Similar "surface explosions" and associated water production have also been reported experimentally during the reduction of NO_2 [35]. A recent theoretical investigation of the N_2O+H_2 reaction on Ir(110) reveals that this system is also characterized by bistability [27]. These examples comfort us in the idea that explosive transients, which in our approach should be associated with an underlying bistability, could be a generic feature of the type of reactive systems we consider here. The explosive

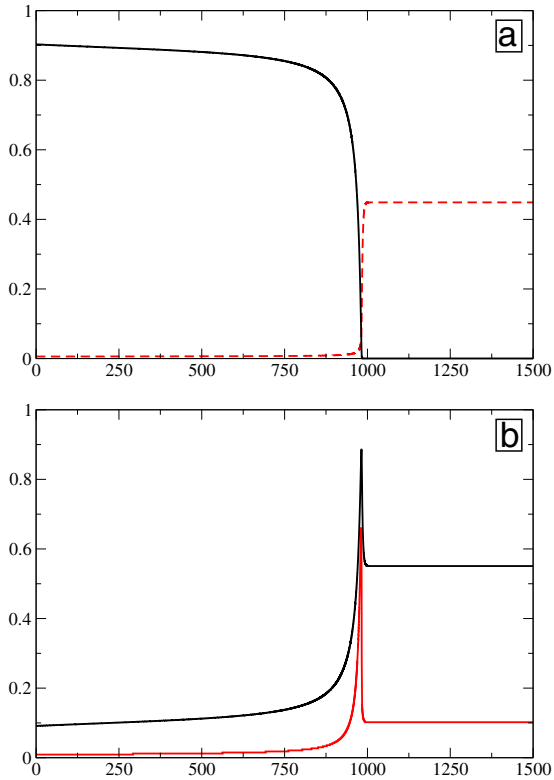

Fig. 3. (Color online) Temporal evolution obtained by numerical integration of equations (4)–(5) in the limit of a perfectly mixed system. The figures depict respectively (a) the coverages in X (plain curve) and H (dashed curve) and (b) the fraction of empty sites (plain curve) and (10×) the reaction rate (dashed curve). In these figures, $k_1\, p_X = 0.0185\ s^{-1}$ with all the other parameters identical to those in Figure 2, $x(0) = 0.903$ and $h(0) = 0.006$.

dynamics generated by our model is depicted in Figure 3 in the case of a well-mixed system. We may note that the main characteristics of the experiments are recovered: the system remains for a long time in a highly X-covered and inactive state and then suddenly switches to a state of high reactivity.

When considering spatially distributed systems, one may note that the transition can be accompanied by a specific spatiotemporal development for appropriate initial conditions. When the initial surface is a randomly perturbed β state, the transition to the final α state takes place in a homogeneous way. On the other hand, starting with a nucleus of the active state inside an otherwise inactive surface, the transition is characterized by a "front" propagating at an almost constant velocity (Fig. 4). Note that the reaction rate is especially strong at the level of the interface between the initial and final states, where the surface is almost empty. Because of this, such a propagation is observed only when the diffusion of X is not too fast; if it is not the case, this adsorbate diffuses rapidly into the pro-reactive nucleus and the surface rapidly becomes homogenous. It is worth noting that similar ring-shaped propagating activity was observed in several experiments of field ion (or electron) microscopy involving the type of systems studied here [32–35].

Fig. 4. Spatial propagation of the reactive state in two dimensions: all the parameters are the same as in Figure 3, with now $D_X = 0.01\ s^{-1}$ and $D_H = 1\ s^{-1}$. The initial condition consists of an empty patch of diameter = 1 in an otherwise X-covered surface of linear size $L = 10$. Blank regions correspond to high reaction rates and dark ones to inactive regions. The time is respectively 10, 30 and 50.

Despite its simplicity the model is thus able to reproduce the main qualitative features of the experimental observations, namely bistability and the existence of explosive transients of high reactivity emerging from an inactive, highly X-covered surface. The observed explosions can from this point of view be interpreted as reaction-induced transitions from an almost poisoned surface toward a reactive state, taking place in the vicinity of a bifurcation point. The rapidity of the transition can be traced back to the autocatalytic character of the third step of our lumped model: as soon as a sufficient number of empty sites appear, this rapid process can ignite and produce even more empty sites.

3 Stochastic description

Our main objective here is to assess the validity of the MF description, with respect to the dynamics generated when taking into account the (spontaneous) fluctuations of composition in the system. To do this, we consider the elementary events as Markov processes, so that a master equation can be written for the underlying surface state probabilities. In this section, we first describe the basic properties of such a master equation, the form of the transition probabilities and the "exact" evolution equations which can be deduced for the coverages. We show how the MF approximation corresponds to the mass-action law discussed in the previous section, and how to obtain evolution equations which account for the microscopic dynamics. We also present the corresponding simulation procedure (Kinetic Monte Carlo simulations).

3.1 Master equation and evolution equations

We will adopt here a lattice gas representation of the adsorbate/surface system. The surface is pictured as a lattice whose nodes correspond to the active sites of the underlying solid surface. Each node located at $\mathbf{r}$ is characterized by a set of local occupation numbers $\{n_j(\mathbf{r},\tau)\}$ at any time τ which are equal to one if the site is occupied by species j (being X, H or *) and equal to zero otherwise. The ensemble $\mathbf{n} = \{n_j\}$ of all local occupation numbers defines the configuration of the surface at any time. We

now use τ for time to avoid confusion with the t used in the mass-action laws. Only square isotropic lattices will be considered.

The different steps of the reactive scheme are assimilated to Markov processes, so that the time evolution of the probabilities in the (surface) states space is given by the following Glauber master equation

$$\frac{d}{d\tau}\,p(\mathbf{n},\tau) = \sum_{\mathbf{n}'\neq\mathbf{n}}\sum_{\rho}\sum_{\mathbf{r}}\left[w_\rho^{\mathbf{r}}(\mathbf{n}'\to\mathbf{n},\tau)\,p(\mathbf{n}',\tau) - w_\rho^{\mathbf{r}}(\mathbf{n}\to\mathbf{n}',\tau)\,p(\mathbf{n},\tau)\right]. \tag{6}$$

In this equation, $p(\mathbf{n},\tau)$ is the probability to find the surface in the configuration $\mathbf{n}$ at time τ. Since we are considering a set of reactions $\{\rho\}$ changing the local configuration of the surface, the global transition probabilities are given in terms of local transition probabilities $w_\rho^{\mathbf{r}}$. The evolution laws for the moments of the underlying probability distribution can be derived from (6) if the transition probabilities are explicitly known.

These different transition probabilities must reflect the mechanistic details of the considered event and must respect detailed balance at equilibrium. The adsorption and desorption of X being molecular, these steps will for example involve only the local occupation of one active site:

$$w^{\mathbf{r}}_{\mathrm{ads,\,X}} = P^{\mathrm{X}}_{\mathrm{ads}}\,n_*(\mathbf{r},\tau); \quad w^{\mathbf{r}}_{\mathrm{des,\,X}} = P^{\mathrm{X}}_{\mathrm{des}}\,n_{\mathrm{X}}(\mathbf{r},\tau)$$

where $P^{\mathrm{X}}_{\mathrm{ads}}$, $P^{\mathrm{X}}_{\mathrm{des}}$ are constants. For the sake of readability, we do not note explicitly the global configurations in the transition probabilities anymore. The case of H_2 is slightly different: its adsorption is known to be dissociative and its desorption recombinative on most transition metals. These two steps thus necessitate that, respectively, two randomly chosen adjacent (first neighbor) empty sites or adjacent H be present, which leads to

$$w^{\mathbf{r}}_{\mathrm{ads,\,H_2}} = \frac{P^{\mathrm{H_2}}_{\mathrm{ads}}}{4}\,n_*(\mathbf{r})\sum_{\mathbf{r}'}n_*(\mathbf{r}'),$$

$$w^{\mathbf{r}}_{\mathrm{des,\,H_2}} = \frac{P^{\mathrm{H_2}}_{\mathrm{des}}}{4}\,n_{\mathrm{H}}(\mathbf{r})\sum_{\mathbf{r}'}n_{\mathrm{H}}(\mathbf{r}')$$

where the sum runs over the first neighbors of $\mathbf{r}$. The reactive step itself is also constructed in accordance with the chosen microscopic mechanism: the site where the X molecule will deposit the oxygen must be an adjacent empty site. The two H adatoms, which are necessary for the formation of H_2O must in consequence be themselves first neighbors of the empty site where the oxygen arrives, leading to a transition probability of the form

$$w^{\mathbf{r}}_{\mathrm{reac}} = \frac{P_{\mathrm{reac}}}{4}\,n_{\mathrm{X}}(\mathbf{r})\sum_{\mathbf{r}'}\prod_{\mathbf{r}'',\,\mathbf{r}'''}\left[n_*(\mathbf{r}')n_{\mathrm{H}}(\mathbf{r}'')\,n_{\mathrm{H}}(\mathbf{r}''')\right]$$

with, as mentioned, $\mathbf{r}'$ and $\mathbf{r}'',\mathbf{r}'''$ being first neighbors of $\mathbf{r}$ and $\mathbf{r}'$, respectively. The mechanism of these elementary processes is pictured in Table 1. As for the diffusion of the adsorbates, we will simply consider the traditional point

Table 1. The different adsorption-desorption and reactive elementary steps. H is grey (blue online) and X is black.

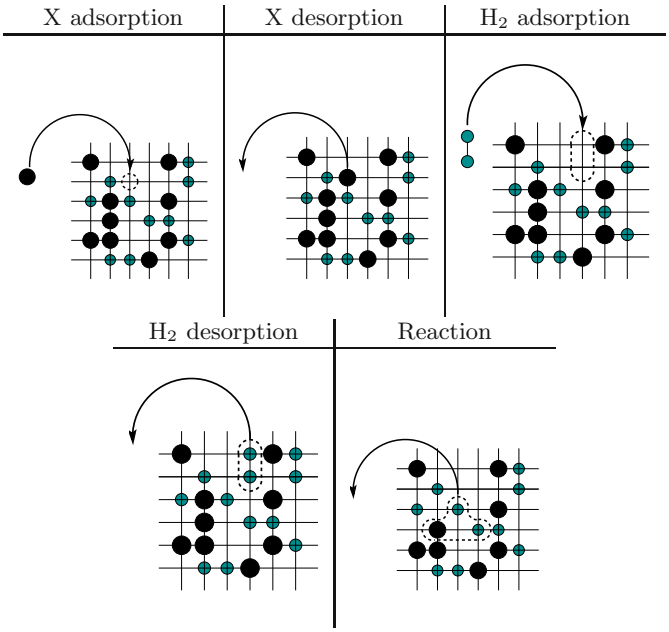

of view stating that the adsorbed molecules perform a random walk by jumping on the available (first neighbors) empty sites, so that

$$w^{\mathbf{r}}_{\mathrm{diff,\,i}} = \frac{P^{i}_{\mathrm{diff}}}{4}\sum_{\mathbf{r}'}\left[n_i(\mathbf{r}')\,n_*(\mathbf{r}) + n_i(\mathbf{r})\,n_*(\mathbf{r}')\right],$$

i being X or H.

The explicit knowledge of the transition probabilities allows for the derivation of "exact" evolution equations for the local occupation probabilities. Note that since the substrate is isotropic, translational invariance should hold for the system under consideration if the initial conditions are random[2] so that the *local* occupation probabilities can also be seen as *global* occupation probabilities, i.e. as global coverages. Noting $\langle ijk\ldots\rangle(\tau)$ the (space-independent) ensemble average of the local configuration $ijk...$, we get

$$\frac{d}{d\tau}\langle \mathrm{X}\rangle(\tau) = P^{\mathrm{X}}_{\mathrm{ads}}\langle *\rangle - P^{\mathrm{X}}_{\mathrm{des}}\langle \mathrm{X}\rangle - 3P_{\mathrm{reac}}\left\langle \begin{array}{ccc} & \mathrm{H} & \\ \mathrm{X} & * & \mathrm{H}\end{array}\right\rangle \tag{7}$$

$$\frac{d}{d\tau}\langle \mathrm{H}\rangle(\tau) = 2P^{\mathrm{H_2}}_{\mathrm{ads}}\langle **\rangle - 2P^{\mathrm{H_2}}_{\mathrm{des}}\langle \mathrm{HH}\rangle - 6P_{\mathrm{reac}}\left\langle \begin{array}{ccc} & \mathrm{H} & \\ \mathrm{X} & * & H\end{array}\right\rangle. \tag{8}$$

These equations clearly illustrate that the evolution in time of the surface concentrations is dictated by the presence of very specific local configurations of particles. It should be noted that the diffusion terms do not appear as such in these evolution equations.

[2] This will, actually, always be the case in our study.

Equations (7)–(8) do not form a closed system since they involve the concentrations of clusters, for which evolution laws are also needed. These evolution laws themselves will include concentrations of bigger clusters, and so on. In order to close this actually infinite hierarchy of equations, some approximation should be made. The simplest of them consists in considering that the probability to find any configuration on the network is simply given by the product of local occupation probabilities. When doing this, we note that the evolution equations form a closed system corresponding in fact to the mass-action equations in the case of a well-mixed surface, if one imposes some connection between the probabilities and the reaction rate constants: $P^{\mathrm{X}}_{\mathrm{ads}} = k_1\, p_{\mathrm{X}}/K$, $P^{\mathrm{X}}_{\mathrm{des}} = k_{-1}/K$, $P^{\mathrm{H_2}}_{\mathrm{ads}} = k_2\, p_{\mathrm{H_2}}/K$, $P^{\mathrm{H_2}}_{\mathrm{des}} = k_{-2}/K$, $P_{\mathrm{reac}} = k_3/3\,K$ where K is some normalization constant ($\tau = K\,t$). This connection is essential in order to compare the time scale of processes arising from the stochastic approach, as compared to the mass-action laws. A connection also exists between the diffusion coefficients and hopping probabilities in the case of isotropic square lattices: $D_i = \Gamma_i\, a^2/4$ where Γ_i is the hopping probability per unit time and a is the lattice constant (the distance between two adjacent sites). In consequence, $P^{\mathrm{X}}_{\mathrm{diff}} = \Gamma_{\mathrm{X}}/K$, $P^{\mathrm{H}}_{\mathrm{diff}} = \Gamma_{\mathrm{H}}/K$ since the a^2 factor simply comes from the transition to continuous coordinates.

The above assumption actually amounts to assuming a complete statistical independence between the local occupation probabilities, i.e. the total absence of spatial correlations between adsorbates. This approximation is usually a crude one for lattice systems and we can already expect it not to hold in our case. A more sophisticated approach consists in taking explicitly into account spatial correlations by including the evolution equations for, e.g., pairs of adsorbates. These evolution laws can then be closed by expressing the probability to find large clusters as a function of lower-order probabilities. For low-dimensional systems, the Kirkwood approximation scheme often gives good results. It consists in factorizing cluster probabilities as $\langle ijk\ldots xyz\rangle \approx \langle ij\rangle\langle jk\rangle\ldots\langle xy\rangle\langle yz\rangle/\langle j\rangle\langle k\rangle\ldots\langle x\rangle\langle y\rangle$ and has been applied sucessfully to a variety of surface reactions. Using this approximation, we get in our case the following evolution equations:

$$\frac{d}{d\tau}\langle \mathrm{X}\rangle(\tau) = P^{\mathrm{X}}_{\mathrm{ads}}\langle *\rangle - P^{\mathrm{X}}_{\mathrm{des}}\langle \mathrm{X}\rangle - 3P_{\mathrm{reac}}\frac{\langle \mathrm{X}*\rangle\langle *\mathrm{H}\rangle^2}{\langle *\rangle^2} \tag{9}$$

$$\frac{d}{d\tau}\langle \mathrm{H}\rangle(\tau) = 2\,P^{\mathrm{H_2}}_{\mathrm{ads}}\langle **\rangle - 2\,P^{\mathrm{H_2}}_{\mathrm{des}}\langle \mathrm{H\,H}\rangle - 6P_{\mathrm{reac}}\frac{\langle \mathrm{X}*\rangle\langle *\mathrm{H}\rangle^2}{\langle *\rangle^2} \tag{10}$$

$$\frac{d}{d\tau}\langle \mathrm{X\,X}\rangle(\tau) = 2\,P^{\mathrm{X}}_{\mathrm{ads}}\langle **\rangle - 2\,P^{\mathrm{X}}_{\mathrm{des}}\langle \mathrm{X\,X}\rangle - \frac{9}{2}\,P_{\mathrm{reac}}\,\frac{\langle \mathrm{X\,X}\rangle\langle \mathrm{X}*\rangle\langle *\mathrm{H}\rangle^2}{\langle \mathrm{X}\rangle\langle *\rangle^2} + \frac{3}{2}\,P^{\mathrm{X}}_{\mathrm{diff}}\left[\frac{\langle \mathrm{X}*\rangle^2}{\langle *\rangle} - \frac{\langle \mathrm{X\,X}\rangle\langle \mathrm{X}*\rangle}{\langle \mathrm{X}\rangle}\right] \tag{11}$$

which form a closed set provided that the diffusion of H is much faster than the other elementary processes (see Appendix B for details). It should be noted that in these equations, the probabilities to find pairs of particles enter explicitly as dynamical variables and are not simply given by the product of local occupation probabilities, i.e. short-ranged spatial correlations between X particles are now taken into account.

One of our main goals will be to compare the validity of the MF and Kirkwood descriptions with respect to the "exact" stochastic dynamics generated by the master equation. We will thus now rapidly summarize the procedure we used to simulate the aforementioned stochastic processes.

To simulate these out-of-equilibrium stochastic processes, we used Kinetic Monte Carlo simulations based on the following algorithm:

1. The substrate is modeled as a square lattice with periodic boundary conditions, composed of N_0 nodes having a coordinancy of 4. Each of these nodes can be empty, occupied by X or by H. A probability P_i is associated with each of the elementary steps of the scheme and an initial configuration of the lattice is chosen (corresponding to a random distribution of the adsorbates).
2. One site is chosen at random: its composition and local environment are then analyzed and one of the processes is selected (with the appropriate probability P_i). If the microscopic configuration is in accordance with the chosen process, the composition of the surface is changed. To be more precise,
   - for the adsorption (desorption) of X, the site must initially be empty (occupied by X) and becomes occupied by X (becomes empty);
   - if H_2 adsorption (desorption) has been selected, the site and one randomly chosen first neighbor must be empty (occupied by H). If this is the case, the two chosen sites become occupied by 2H (or become empty);
   - for the reaction itself, the randomly chosen site must be a X and one randomly chosen first neighbor must be empty. If in addition two of the first neighbors of the empty site are occupied by H, the reaction takes place and all the involved nodes are emptied;
   - in the case of diffusion, a pair of first neighbors is randomly picked up. If the diffusion of X has been selected, it will take place if one of the sites is X and the other one is empty: X then jumps toward its neighbor. The diffusion of H is treated in a similar way;
3. Whatever the process, and whatever the result of the corresponding attempt, time is advanced by $1/N_0$ and the algorithm goes back to 2.

It should be noted that the implementation of these types of simulations requires the normalization of the probabilities P_i used in the definition of the transition probabilities. Given their connection with the different rate

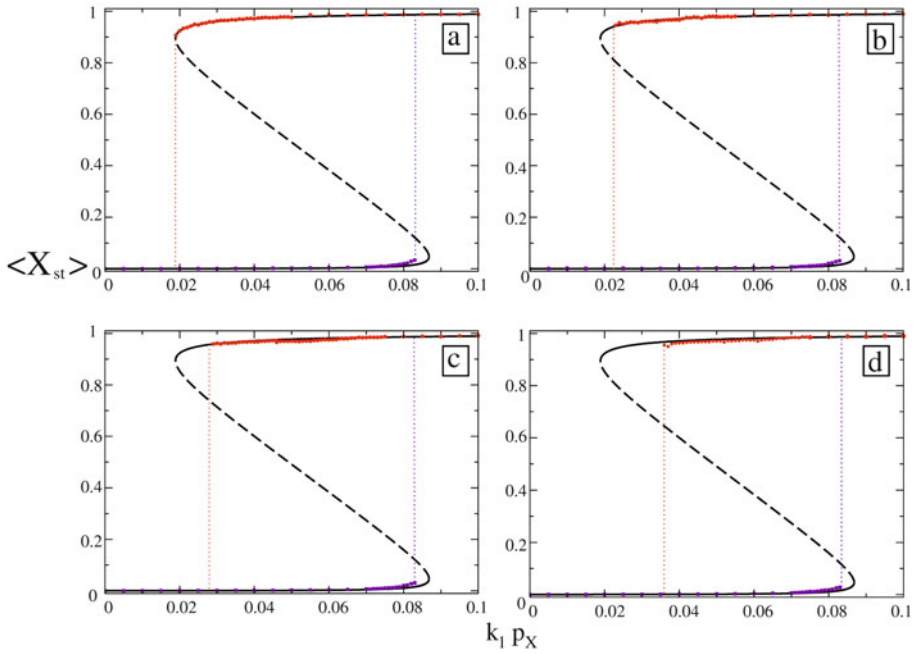

Fig. 5. (Color online) Steady states diagram given by KMC simulations, with all kinetic parameters being identical to those of Figure 2. The hydrogen hopping frequency $\Gamma_{\mathrm{H}} = 10^3$ s^{-1}, and Γ_{X} is equal to (a) 1, (b) 0.1, (c) 0.01 and (d) 0.001 s^{-1}, respectively.

constants, this implies that the normalization constant reads $K = k_1\, p_{\mathrm{X}} + k_{-1} + k_2\, p_{\mathrm{H}_2} + k_{-2} + k_3/3 + \Gamma_{\mathrm{X}} + \Gamma_{\mathrm{H}}$.

4 Simulations

In this section, we show the main features of the system properties obtained from KMC simulations and compare them with the predictions made in the MF limit. We first focus on the steady states and subsequently on the spatiotemporal kinetics.

4.1 Stationary properties

To characterize the stationary properties of the microscopic system, we have performed a large amount of simulations (from 500 to 1000 realizations) over very long times (usually the simulation time was $\tau = 10\,000$), allowing us to evaluate the ensemble averages for coarse variables such as global coverages. The initial conditions consist in randomly adsorbed particles with a prescribed initial macroscopic coverage, as detailed in the simulations procedure. The existence of steady-state multiplicity was tested by varying the initial coarse surface composition while keeping all the parameters constant.

To illustrate how the mobility of X can affect the steady state properties, we plot in Figure 5 the stationary global X coverages for different numerical values of Γ_{X} with all the other parameters being the same as in Figure 2. When the mobilities of both reactants are high (and the system is sufficiently large), the mass-action laws predictions about the steady state values and the parametric zone of bistability are recovered, as expected (Fig. 5a). Small differences are still observed in a close neighborhood of the bifurcation points, where the amplitude of fluctuations is known to diverge. Using large values of the H hopping probabilities is consistent with the available experimental data, as surface diffusion of hydrogen atoms is known to be rapid on most metallic facets. The mobility of X can however be fairly low, especially at low temperatures, in the case of large molecules or if a strong binding exists between the metal and some of the atoms in X [29]. In the limit of low X mobility, we may note that despite the rapid diffusion of adsorbed hydrogen atoms, strong deviations from the previous predictions can be observed. More precisely, one can notice in this case that the bifurcation point $p^{(1)}$ is displaced towards a higher value. The other turning point, $p^{(2)}$, does not seem to be strongly affected by the mobility of X, which is not surprising as the coverage of this species is there almost zero. All in all, this situation leads to an effectively reduced zone of bistability.

Deviations from the mean field steady state are recurrent in nonlinear reactive lattice systems, and can typically be attributed to the emergence of spatial correlations between adsorbed particles. To quantify this in our case, let us consider for example the spatial covariance between adsorbates, defined as

$$\begin{aligned} C_{ij} &= \langle \delta n_i(\mathbf{r},t)\, \delta n_j(\mathbf{r}',t)\rangle \\ &= \langle n_i(\mathbf{r},t) n_j(\mathbf{r}',t)\rangle - \langle n_i(\mathbf{r},t)\rangle\, \langle n_j(\mathbf{r}',t)\rangle, \end{aligned}$$

where $\mathbf{r}$ and $\mathbf{r}'$ are the (discrete) coordinates of two first neighbors on the lattice. These functions are representative of the level of spatial coherence between particles i

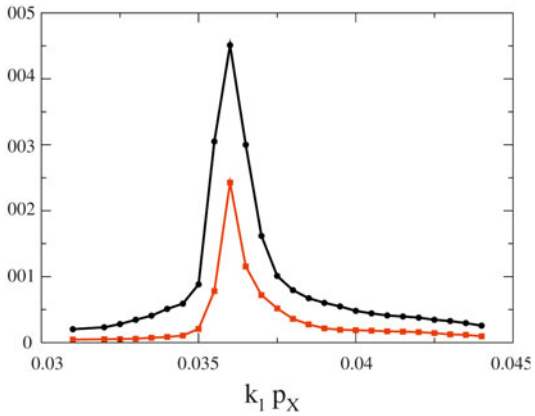

Fig. 6. (Color online) Steady state spatial covariance in the β state between adsorbed X molecules (circles) and between empty sites (squares), obtained for parameter values identical to those of Figure 5d. Large correlations are observed in the vicinity of the turning point $p^{(1)}$.

and j. Indeed, if two species are distributed completely randomly on the lattice, C_{ij} is strictly zero, while positive or negative values are on the contrary indicative of a tendency for i and j particles to form aggregates or to occupy separate regions of the surface, respectively. In our case, as shown in Figure 6, the steady state spatial covariances take especially large values whenever strong deviations from the mass-action law are observed, indicative of the existence of strong, short-ranged spatial correlations in the inactive β state. These correlations are especially strong between adsorbed X particles and between empty sites, while H adatoms are so to say spatially uncorrelated (their spatial covariance remains flat throughout the whole diagram and is thus not represented). The stationary β state is thus characterized by a specific spatial compartmentalization of the surface, where X particles and empty sites tend to occupy different subregions while H is homogeneously distributed. Since X is the major species, this configuration in fact corresponds more or less to a highly X-covered surface with small holes in it.

Since the observed deviations can be related to the emergence of short-range spatial correlations, one should expect that theories such as the Kirkwood approximation would lead to a better description of the steady state properties. In order to verify this, a comparison has been made between the MF approach, KMC simulations and the Kirkwood approximation (Eqs. (9)–(11)): the corresponding steady states are depicted in Figure 7. One may note that the simulations and the amended evolution equations lead to almost identical steady state values for the average coverages: in particular, the localization of the poisoned state and the bifurcation point $p_{\mathrm{X}}^{(1)}$ are very close, especially in comparison with the MF results. The second bifurcation point is, on the other hand, not estimated with a high precision by the Kirkwood scheme; this is due to the fact that we completely neglect correlations between H particles in such an approach. It is worth noting that a similar displacement of bifurcation points has been observed for other systems, such as kinetic models for the $CO+O_2$ reaction on Pt(001) [37]. The modification of the steady states was interpreted then as a change in the relative stability between a CO-poisoned inactive state and a coexisting CO-poor reactive state, which are very similar to the states encountered here.

The Kirkwood approximation furthermore offers a nice and simple explanation as to why a high mobility can restore the MF dynamics. In this approach, the hopping probabilities do not appear in the evolution equations for the first moments (the average coverages): this doesn't mean of course that the dynamics is not diffusion-dependent. $P_{\mathrm{diff}}^{\mathrm{X}}$ indeed appears in the evolution equations for the second moments (see Eq. (11)), so that the effective kinetics will depend on how the diffusion acts on the evolution of higher order moments. We may note for example that, if $P_{\mathrm{diff}}^{\mathrm{X}}$ takes large values, the evolution law for the probability to find pairs of X takes the form

$$\frac{d}{d\tau}\langle \mathrm{X}\,\mathrm{X}\rangle(\tau) \approx P_{\mathrm{diff}}^{\mathrm{X}}\left[\frac{\langle \mathrm{X}*\rangle^2}{\langle *\rangle} - \frac{\langle \mathrm{X}\,\mathrm{X}\rangle\langle \mathrm{X}*\rangle}{\langle \mathrm{X}\rangle}\right].$$

Since in this limit $P_{\mathrm{diff}}^{\mathrm{X}}$ is much larger than any of the other event probabilities, this pair probability evolves on time scales which are much faster than the ones associated with $\langle \mathrm{X}\rangle$ or $\langle \mathrm{H}\rangle$, whose dynamics does not depend explicitly on the hopping probabilities. The important time scale separation allows us to estimate that $\langle \mathrm{X}\,\mathrm{X}\rangle$ rapidly reaches a quasi-steady state characterized by

$$\frac{\langle \mathrm{X}*\rangle^2}{\langle *\rangle} \approx \frac{\langle \mathrm{X}\,\mathrm{X}\rangle\langle \mathrm{X}*\rangle}{\langle \mathrm{X}\rangle}$$

which leads to

$$\langle \mathrm{X}\,\mathrm{X}\rangle \approx \langle \mathrm{X}*\rangle\frac{\langle \mathrm{X}\rangle}{\langle *\rangle} \approx \langle \mathrm{X}\rangle^2.$$

The latter relation amounts to validating the MF assumption, which stipulates a perfect statistical independence between adsorbed particles. In other words, when the mobility of the particles is large enough, higher moments become "slaved" to the relatively slow evolution of the first, dominant moments so that the MF evolution laws can be seen as the result of an adiabatic elimination of the rapidly evolving high moments, due to large values of hopping probabilities. It should finally be emphasized that further comparison between simulations and evolution equations reveal that the performance of the Kirkwood approximation scheme is good only as long as the mobility of X is not too close to zero. For very low hopping probabilities of the monomer, even the amended evolution laws become indeed unsatisfactory because, as revealed by simulations (but not shown here), long-ranged spatial correlations tend to become non-negligible.

Deviations from the MF predictions are mostly observed in the vicinity of the turning point originating from the quasi-poisoned state. Since the explosive transitions corresponding to those observed in experiments take place in the same parametric region, one could wonder whether these transients are influenced by the inhomogeneous fluctuations and consequent spatial correlations. We will thus

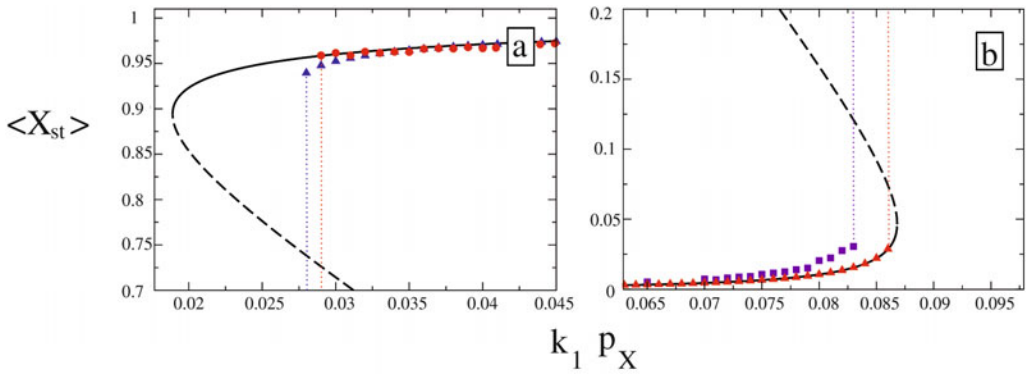

Fig. 7. (Color online) Stationary coverages corresponding to (a) an initially X-poisoned surface and (b) an initially empty system. The plain and dashed curves correspond to the mass-action law predictions (stable and unstable states, respectively) and triangles to those of the Kirkwood approximation scheme. Simulation results are represented by circles (a) and squares (b). For these figures, $\Gamma_{\rm H} = 10^5$ s^{-1}, $\Gamma_{\rm X} = 0.01$ s^{-1} (all other parameters being the same as before).

focus now on the spatiotemporal development of these phenomena as obtained by simulations.

4.2 Spatiotemporal development of explosive transients

As discussed in Section 2, explosive transitions are observed in the MF kinetic description when the surface is initially close to (but outside) the zone of existence of the inactive state. In this section, we focus on how fluctuations and spatial correlations can alter the MF picture of these transient behaviors.

If the mobility of X is sufficiently large, explosive transients are observed in simulations which are very similar to those predicted by the MF. The intrinsic fluctuations of composition however induce a statistical distribution of the ignition time of the explosive transients from one realization to the other (see for example Fig. 8). Note that a distribution of the ignition time of surface explosions has been reported in the literature for several systems of the class we consider here (such as the NO+H_2 reaction [15] or the decomposition of acetates [28]). The dispersion of the ignition time becomes larger when the system is small or placed close to the bifurcation point; these two trends are in fact expected in homogenous explosive systems submitted to noise [3].

Just like for steady state properties, important deviations from this MF-like behavior are observed when the mobility of the monomer species is low. To illustrate this, we have plotted in Figure 9 (average) transitions for different values of $\Gamma_{\rm X}$. Two important trends can be highlighted. First, the mean ignition time of the explosions tends to become shorter as one considers lower and lower diffusion probabilities for X. Second (but not shown here), the dispersion of the ignition time also gets narrower when considering the same limit. These observations are in line with the displacement of the critical pressure $p^{(1)}$ delimiting the zone of existence of the quasi-poisoned state. The initial condition that was chosen in Figure 9 actually corresponds to larger and larger distances from criticality as

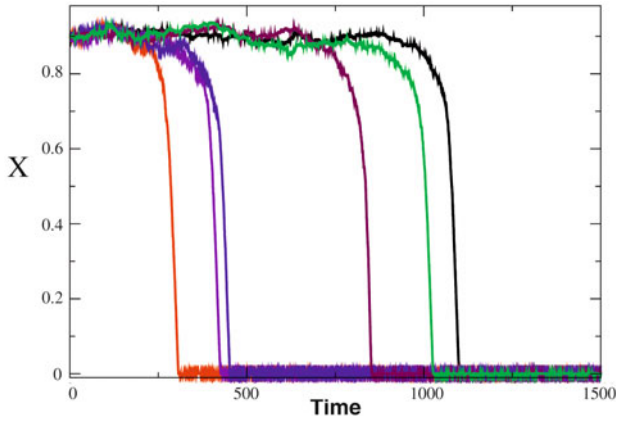

Fig. 8. (Color online) Realizations of explosive transitions starting from an almost poisoned state ($x(0) = 0.9$, $h(0) = 0.005$): time evolution of the spatially averaged number of X particles. The parameters are: $k_1\, p_{\rm X} = 0.19$ s^{-1} (the critical value being 0.2), $k_{-1} = 0.001$ s^{-1}, $k_2\, p_{\rm H_2} = 0.1$ s^{-1}, $k_{-2} = 0.1$ s^{-1} and $k_3 = 300$ s^{-1}, $\Gamma_{\rm X} = 1$ s^{-1}, $\Gamma_{\rm H} = 10^3$ s^{-1} for this system of size $N_0 = 1000$.

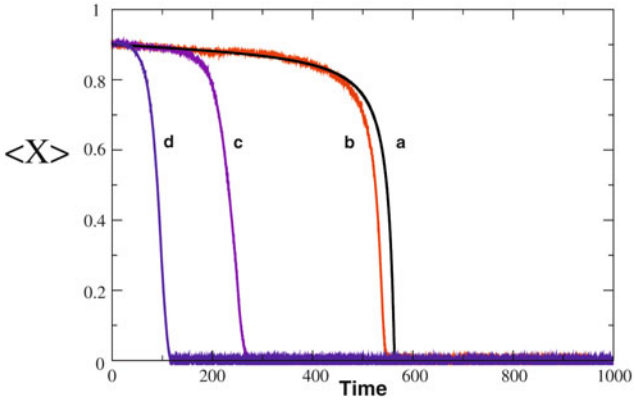

Fig. 9. (Color online) Average (500 realizations) for initial condition and parameter values identical to those of Figure 8, except for $\Gamma_{\rm X}$, being respectively (b) 10, (c) 0.1 and (d) 0.001 s^{-1}. The curve (a) corresponds to the MF prediction.

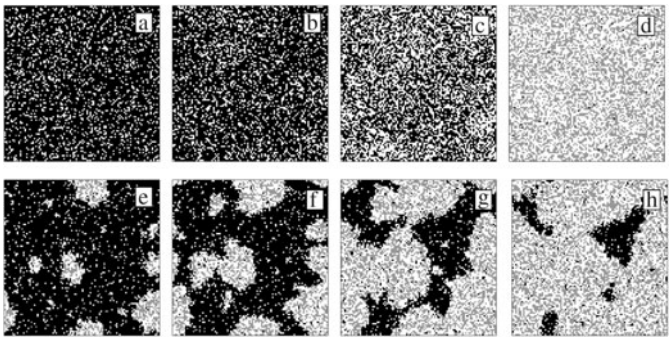

Fig. 10. Snapshots taken during the explosive transient corresponding to curve (b) in Figure 9a–9d and to curve (d) in the same figure (e–h). The size of the system is 100×100.

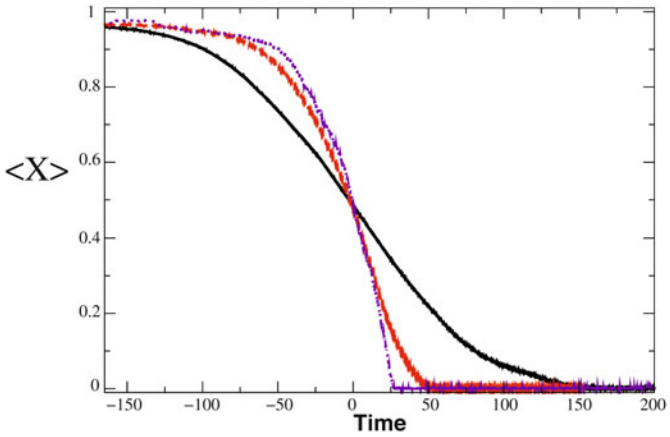

Fig. 11. (Color online) Temporal evolution of average X coverage, obtained from a single simulation realization. The parameters are the same as in Figure 9d, except for $k_1\, p_X = 0.35\ s^{-1}$. The transitions have been centered on their respective ignition times for an easier comparison between profiles. The size of the system is respectively $N_0 = 10^5$ (plain curve), $N_0 = 10^4$ (dashed curve) and $N_0 = 10^3$ (dotted curve).

Γ_X is decreased. Since the mean ignition time is expected to scale as $t_{ign} \sim |k_1\, p_X - p^{(1)}|^{-1/2}$, it is indeed supposed to increase when decreasing Γ_X. In parallel, the amplitude of fluctuations is known to decrease as the system is placed further from a critical point, which gives a first explanation as to why dispersion in the ignition times tends to decrease.

It should be emphasized at this stage that both the stationary and transient properties are modified in the limit of low mobility in such a way that the reactive state seems to be favored in comparison with the inactive one. It could seem surprising, at first glance, that the lack of efficient mixing actually *enhances* the effectiveness of a reaction. The key to this trend lies in the intrinsically autocatalytic aspect of the nonlinear X decomposition. To illustrate this, we have plotted in Figure 10 snapshots of the surface composition during explosive transients for rapidly and slowly diffusing X (Figs. 10a–10d and 10e–10h, respectively). In these pictures, X particles appear black, H is grey and empty sites are blank. After a reactive event, the surface is locally emptied because of the immediate desorption of the products. On one hand, if the mobility of the adsorbates is high, surrounding particles (here, the monomer) can invade this empty patch and the local depletions are rapidly diluted in the system, which remains more or less homogeneous (see Figs. 10a–10d). On the other hand, if the mobility of the monomer is low, a "hole" is created in the coverage where all surrounding X can decompose (Figs. 10e–10h). The lack of efficient mixing thus acts so that pro-reactive local fluctuations are maintained and subsequently propagate towards the rest of the system, instead of being washed out by diffusion. It should be emphasized that such a propagation is also observed in the case of immobile reactants, which is a sign that at least part of the propagation is induced by the non-locality of the reactive events, as discussed for example in [38] and [39,40].

The dynamics of surface explosion is thus governed by a "nucleation and growth"-like mechanism of the reactive state in an inactive one, in the limit of low X mobility. The clusters which are formed are initially composed of only several particles, in other words well beyond the limits of applicability of the MF assumption. Because the formation of these patterns takes place at small scales, one can observe strong size effects in the development of the explosive transients. As pictured in Figure 11, single transitions from an (almost) poisoned state to the α state are usually quite sharp for relatively small surfaces, since the clusters rapidly invade the whole system. However, for identical conditions the same transition is much smoother for larger systems and the observed transient can in fact barely be named "explosive". This lack of *global* explosivity, despite rapid *local* transitions can clearly be related to a problem of synchronization between the different parts of the system: different clusters are created at different times and different locations, leading to an inhomogeneous, globally unsynchronized behavior (see also Figs. 10e–10h). It seems thus that a subtle connection exists between the dynamics at different scales, which can lead to a large-scale behavior being quite different from short-scale ones. It should be noted that the Kirkwood approximation is not really efficient in reproducing these tendencies. The Kirkwood approach underestimates the deviations from the MF approximation: these discrepancies can be traced back to the neglecting of long-range spatial correlations which appear during the transition (but are not present at the steady state).

5 Conclusions

In this paper, we have investigated a simple model of surface reaction where the decomposition of some adsorbates into oxygen is followed by the rapid formation of water, due to the presence of coadsorbed hydrogen. We have compared the dynamics obtained in the "traditional" reaction-diffusion description with a mesoscopic and stochastic

approach, taking explicitly into account fluctuations and spatial correlations. Our work has revealed that the mass-action law is in many circumstances unable to correctly predict the spatiotemporal development of the considered class of reactive systems.

Discrepancies are observed both for transients and stationary states. The traditional kinetic approach correctly predicts the presence of a bistability between a X-poisoned surface and a much more reactive (and relatively empty) state, which is induced by the intrinsically autocatalytic character of X decomposition. However, the localization of the steady states and the turning points are consistent with simulation results only in the limit where both adsorbates diffuse very fast compared with other processes. In more realistic situations, it appears that the mass-action law becomes inappropriate and for example underestimates the efficiency of the decomposition step and consequently overestimates the region of existence of the poisoned state. These observations are consistent with other studies on the role played by the mobility of adsorbates on the accuracy of the mean field approach.

The reaction-diffusion equations also predict, in the vicinity of one of the turning points, the existence of explosive transients which are very similar to those observed in experiments. Once more, this prediction seems to hold only in the limit of rapidly diffusing adsorbates. When the mobility of one of the adsorbates becomes low, the macroscopic explosivity of the transition is lost in simulations. To our knowledge, such a loss of explosivity had not been reported before but could well be observed in many surface reactions. It should also be noted that, in opposition to the results obtained through simulations, the traditional reaction-diffusion approach is unable to reproduce the wide dispersion of ignition times observed experimentally in the case of small systems [33,34].

So what is the main reason behind this inefficiency of the traditional reaction-diffusion equations and how could they be amended? In the mean field hypothesis the behavior of a particle can be described as being due to an effective field created by the rest of the system, which is seen as homogeneous. In each of the aforementioned situations, the inefficiency of the mean field approximation in reproducing the simulations results can be traced back to the formation of a short-scale organization of adsorbed particles. These microstructures appear here despite the fact that lateral interactions are not taken into account. They are solely induced by the reaction steps, creating strong spatial correlations between the reactants which are not washed out by diffusion. This results for example in a desynchronization of different regions of the system, which gives a simple explanation for the disappearance of explosions in the limit of low mobility. The deviations arise thus as a consequence of a competition between reaction-induced correlations and diffusion, which tends to suppress them. Fortunately, most of the observed deviations can be reproduced and rationalized by considering explicitly the time evolution for the probability to find pairs of particles, on the basis of the master equation governing the dynamics of the system. This higher order approximation of the dynamics takes into account the existence of spatial correlations between first neighbor adsorbates and is thus not a mean field approach in the sense that spatial correlation functions are non-trivial. This "extended" dynamics reveals itself quite efficient in describing the stationary properties, but is less effective for the explosive transients, during which longer-ranged correlations appear.

In summary, we have shown that the traditional mass-action law description fails to correctly describe the behavior of an important class of autocatalytic surface reactions. This departure should reveal itself for systems where the hopping frequency of an oxygen-rich species is lower than the characteristic frequency of the oxygen-hydrogen combination giving water. Such situations are encountered at relatively low temperatures and/or in the case of molecules binding strongly to the substrate. For example, the propagation velocity of reaction fronts for the H_2+O_2 reaction were shown to deviate substantially from the reaction-diffusion predictions at low temperatures. The traditional equations predicted a front velocity being one order of magnitude slower than experimental observations, contrary to the corresponding Monte Carlo simulations [41]. We believe this could be an effect of a reaction-induced propagation similar to what we describe here, which tends to accelerate the fronts during an autocatalytic transition. In any case, for this type of systems the attribution of a microscopic reaction mechanism based on a comparison between mass-action laws and experimental measurements might prove inadequate.

This work clearly opens new perspectives in the modeling of complex surface reactions. For example, this analysis could be extended to the hydrogenation of large organic molecules on transition metals. It could also be extended to account for strong lateral interactions which are known to induce formation of nanostructures on the surface. In this paper, we showed that small scale structures can also appear simply because of the cooperativity of elementary steps and the constrained geometry of the support. This suggests that a careful study should be done on the possible combination of nonlinearity- and interaction-induced nanoscale pattern formation in surface systems, possibly opening the way to new types of structures. Finally, the inaccuracy of both the mean field and the Kirkwood approximation in the description of the explosive transients suggests that a different approach should be used to model them, such as maybe Avrami-like kinetics that explicitly consider the nucleation-and-growth type of transition observed here [42].

We would like to thank Grégoire Nicolis for the numerous fruitful and useful discussions.

Appendix A

In this appendix we detail the derivation of the diffusion terms appearing in equations (4)–(5), starting from thermodynamical considerations. We start from the chemical

potential of the different species that form here an ideal mixture

$$\mu_{\mathrm{X}}(\mathbf{r},t) = \mu_{\mathrm{X}}^0 + RT\ln\theta_{\mathrm{X}}(\mathbf{r},t)$$
$$\mu_{\mathrm{H}}(\mathbf{r},t) = \mu_{\mathrm{H}}^0 + RT\ln\theta_{\mathrm{H}}(\mathbf{r},t) \quad (A.1)$$
$$\mu_{*}(\mathbf{r},t) = \mu_{*}^0 + RT\ln\theta_{*}(\mathbf{r},t) \quad (A.2)$$

where θ is the local coverage of the species of interest and θ_* is the local fraction of empty sites. This form of the chemical potential is easily deduced from the local free energy estimated within the framework of the mean field theory applied to equilibrium statistical mechanics.

Diffusion is known to present a large domain of linear response with respect to perturbations from the equilibrium state. In consequence we will consider that the diffusive flux (diffusion with respect to empty sites) is simply proportional to the corresponding thermodynamical force, i.e. to the gradient of the difference of chemical potential of the considered species and the species of reference (here, empty sites) [43]. The isothermal diffusive fluxes will thus read in general

$$\mathbf{J}_{\mathrm{X}}^{\mathrm{diff}}(\mathbf{r},t) = -L_{\mathrm{XX}}\left[\frac{\nabla(\mu_{\mathrm{X}}-\mu_*)}{T}\right] - L_{\mathrm{XH}}\left[\frac{\nabla(\mu_{\mathrm{H}}-\mu_*)}{T}\right]$$
$$\mathbf{J}_{\mathrm{H}}^{\mathrm{diff}}(\mathbf{r},t) = -L_{\mathrm{HX}}\left[\frac{\nabla(\mu_{\mathrm{X}}-\mu_*)}{T}\right] - L_{\mathrm{HH}}\left[\frac{\nabla(\mu_{\mathrm{H}}-\mu_*)}{T}\right].$$

As was shown earlier starting from the corresponding master equation, in the case of diffusing hard spheres on a lattice, the cross-diffusion terms are zero as long as there is no direct exchange of hard spheres (i.e. when hopping can only take place between an occupied site and an empty one). In order to estimate L_{XX} and L_{HH}, let us consider the case of a single diffusing species, which should be equivalent to Fick's law, say $\mathbf{J}_{\mathrm{X}}^{\mathrm{diff}}(\mathbf{r},t) = -D_{\mathrm{X}}\nabla\theta_{\mathrm{X}}$, since the adsorbate is a random walker on a lattice (with $D_{\mathrm{X}} = \mathrm{cst}$). We get

$$\mathbf{J}_{\mathrm{X}}^{\mathrm{diff}}(\mathbf{r},t) = -L_{\mathrm{XX}}\left[\frac{\nabla(\mu_{\mathrm{X}}-\mu_*)}{T}\right] = -L_{\mathrm{XX}}\,R\,\frac{\nabla\theta_{\mathrm{X}}}{\theta_{\mathrm{X}}\,\theta_*},$$

since $\theta_* = 1-\theta_{\mathrm{X}}$. As a consequence, $D_{\mathrm{X}} = L_{\mathrm{XX}}\,R/\theta_{\mathrm{X}}\,\theta_* = \mathrm{cst}$, or $L_{\mathrm{XX}} = D_{\mathrm{X}}\,\theta_{\mathrm{X}}\,\theta_*/R$.

The multispecies diffusion equation can then be obtained under the assumption that the diffusion coefficients remain constant even in the presence of additional adsorbates. On this basis, we get for X

$$\mathbf{J}_{\mathrm{X}}^{\mathrm{diff}}(\mathbf{r},t) = -\frac{D_{\mathrm{X}}\,\theta_{\mathrm{X}}\,\theta_*}{R}\left[R\,\frac{\theta_*\,\nabla\theta_{\mathrm{X}} - \theta_{\mathrm{X}}\nabla\theta_*}{\theta_{\mathrm{X}}\,\theta_*}\right] = -D_{\mathrm{X}}\left[\theta_*\,\nabla\theta_{\mathrm{X}} - \theta_{\mathrm{X}}\nabla\theta_*\right].$$

In the case of the two co-adsorbates situation considered here, this becomes

$$\mathbf{J}_{\mathrm{X}}^{\mathrm{diff}}(\mathbf{r},t) = -D_{\mathrm{X}}\left[(1-\theta_{\mathrm{H}})\,\nabla\theta_{\mathrm{X}} + \theta_{\mathrm{X}}\nabla\theta_{\mathrm{H}}\right].$$

because the sum of the coverages is equal to one. This expression for the flux respects several intuitive limits: for example, it tends to zero when $\theta_{\mathrm{X}}+\theta_{\mathrm{H}} \to 1$ (jamming), gives Fick's law when $\theta_{\mathrm{H}} \to 0$, etc. Taking the divergence of this flux, the corresponding diffusion equation for the local coverage of X finally reads

$$\frac{\partial}{\partial t}\,\theta_{\mathrm{X}} = D_{\mathrm{X}}\,\left[(1-\theta_{\mathrm{H}})\,\nabla^2\theta_{\mathrm{X}} + \theta_{\mathrm{X}}\,\nabla^2\theta_{\mathrm{H}}\right]$$

and the same derivation can be done for H. Note that this form of the diffusion equation has also been obtained directly from the master equation for multispecies diffusion of hard spheres under the same assumptions [44,45].

Appendix B

We here detail somewhat the derivation of the evolution laws (9)–(11) taking into account the possible spatial correlations involving X. The time evolution of pair probabilities can be extracted from the Glauber master equation (6) using

$$\frac{d}{dt}\,\langle n_i(\mathbf{r},t)\,n_j(\mathbf{r}',t)\rangle = \langle (n_i(\mathbf{r},t) - 2\,n_i(\mathbf{r},t)\,n_j(\mathbf{r}',t))\sum_\rho w_\rho^{\mathbf{r}'}(\mathbf{n}\to\mathbf{n}',t)\rangle + \langle (n_j(\mathbf{r}',t) - 2\,n_i(\mathbf{r},t)\,n_j(\mathbf{r}',t))\sum_\rho w_\rho^{\mathbf{r}}(\mathbf{n}\to\mathbf{n}',t)\rangle. \quad (B.1)$$

Since each site can have 3 different occupations, there are 9 possible pairs of sites, so that 11 evolution equations are in principle needed within the framework of the Kirkwood approximation scheme. Fortunately, this number can be strongly reduced by taking into account the specificities of the model. First, the translational invariance has the important consequence that the probability to find any pair of sites (say, ij) must respect $\langle i\,j\rangle = \langle j\,i\rangle$, leaving only 6 independent pair probabilities which are moreover linked by conservation relations such as $\langle \mathrm{X}\,*\rangle = \langle \mathrm{X}\rangle - \langle \mathrm{X}\,\mathrm{X}\rangle - \langle \mathrm{X}\,\mathrm{H}\rangle$ or $\langle *\,*\rangle = \langle *\rangle - \langle \mathrm{X}\,*\rangle - \langle *\,\mathrm{H}\rangle$. In addition to this, we can also take into account the fast diffusion of H. A rapid diffusion of this species should lead to the destruction of any reaction-induced correlation between hydrogen and other adsorbates: in terms of probabilities we can thus assume that

$$\langle \mathrm{H}\,\mathrm{H}\rangle \approx \langle *\,*\rangle\,\frac{\langle \mathrm{H}\rangle^2}{\langle *\rangle^2},\ \langle \mathrm{H}\,*\rangle \approx \langle *\,*\rangle\,\frac{\langle \mathrm{H}\rangle}{\langle *\rangle},\ \langle \mathrm{X}\,\mathrm{H}\rangle \approx \langle \mathrm{X}\,*\rangle\,\frac{\langle \mathrm{H}\rangle}{\langle *\rangle}$$
$$\langle \mathrm{X}\,*\rangle \approx \left[\langle \mathrm{X}\rangle - \langle \mathrm{X}\,\mathrm{X}\rangle\right]/\left[1+\langle \mathrm{H}\rangle/\langle *\rangle\right],\ \text{and}$$
$$\langle *\,*\rangle \approx \left[\langle *\rangle - \langle \mathrm{X}\,*\rangle\right]/\left[1+\langle \mathrm{H}\rangle/\langle *\rangle\right] \quad (B.2)$$

so that finally the evolution equation of only one pair configuration is needed. For X pairs, we get

$$\frac{d}{d\tau}\langle \mathrm{X}\,\mathrm{X}\rangle(\tau) = 2\,P^{\mathrm{X}}_{\mathrm{ads}}\,\langle * *\rangle - 2\,P^{\mathrm{X}}_{\mathrm{des}}\,\langle \mathrm{X}\,\mathrm{X}\rangle - \frac{9}{2}\,P_{\mathrm{reac}}\left\langle \begin{matrix} & \mathrm{H} & \\ \mathrm{X} & \mathrm{X} * & \mathrm{H} \end{matrix}\right\rangle + \frac{3}{2}\,P^{\mathrm{X}}_{\mathrm{diff}}\left[\langle \mathrm{X} * \mathrm{X}\rangle - \langle \mathrm{X}\,\mathrm{X} *\rangle\right]. \quad \text{(B.3)}$$

which readily reduces to equation (11), using the Kirkwood approximation and the relations presented in this Appendix.

References

1. R. Imbihl, G. Ertl, Chem. Rev. **95**, 697 (1995)
2. F. Baras, G. Nicolis, M. Malek Mansour, J.W. Turner, J. Stat. Phys. **32**, 1 (1983)
3. P. Peeters, F. Baras, G. Nicolis, J. Chem. Phys. **93**, 7321 (1990)
4. Yu. Suchorski, J. Beben, R. Imbihl, E.W. James, D.J. Liu, J.W. Evans, Phys. Rev. B **63**, 165417 (2001)
5. C. Sachs, M. Hildebrand, S. Völkening, J. Wintterlin, G. Ertl, J. Chem. Phys. **116**, 5759 (2002)
6. S. Völkening, J. Wintterlin, J. Chem. Phys. **114**, 6382 (2001)
7. J. Wintterlin, S. Völkening, T.V.W. Janssens, T. Zambelli, G. Ertl, Science **278**, 1931 (1997)
8. B. Temel, H. Meskine, K. Reuter, M. Scheffler, H. Metiu, J. Chem. Phys. **126**, 204711 (2007)
9. S. Prakash, G. Nicolis, J. Stat. Phys. **82**, 297 (1996)
10. S. Prakash, G. Nicolis, J. Stat. Phys. **86**, 1289 (1997)
11. A. Provata, G. Nicolis, F. Baras, J. Chem. Phys. **110**, 8361 (1999)
12. E.V. Albano, Heter. Chem. Rev. **3**, 389 (1996).
13. R.M. Ziff, E. Gulari, Y. Barshad, Phys. Rev. Lett. **56**, 2553 (1986)
14. R.M. Nieminem, A.P.J. Jansen, Appl. Catal. A **160**, 99 (1997)
15. Y. De Decker, F. Baras, N. Kruse, G. Nicolis, J. Chem. Phys. **117**, 10244 (2002)
16. M.W. Lesley, L.D. Schmidt, Surf. Sci. **155**, 215 (1985)
17. Th. Fink, J.-P. Dath, M.R. Bassett, R. Imbihl, G. Ertl, Surf. Sci. **245**, 96 (1991)
18. Th. Fink, J.P. Dath, R. Imbihl, G. Ertl, J. Chem. Phys. **95**, 2109 (1991)
19. M. Tammaro, J.W. Evans, J. Chem. Phys. **108**, 7795 (1998)
20. L. Vicente, F.V. Caballero, J. Mol. Catal. A: Chem. **272**, 118 (2007)
21. P.D. Cobden, J. Siera, B.E. Nieuwenhuys, J. Vac. Sci. Technol. A **10**, 2487 (1992)
22. M. Slinko, T. Fink, T. Löher, H.H. Madden, S.J. Lombardo, R. Imbihl, G. Ertl, Surf. Sci. **264**, 157 (1992)
23. A.G. Makeev, B.E. Nieuwenhuys, J. Chem. Phys. **108**, 3740 (1998)
24. A.G. Makeev, B.E. Nieuwenhuys, Surf. Sci. **418**, 432 (1998)
25. H. Uecker, R. Imbihl, M. Rafti, I.M. Irurzun, J.L. Vicente, E.E. Mola, Chem. Phys. Lett. **382**, 232 (2003)
26. M. Rafti, J.-L. Vicente, Phys. Rev. E **75**, 061127 (2007)
27. N.V. Peskov, M.M. Slinko, S.A.C. Carabineiro, B.E. Nieuwenhuys, Catal. Today **105**, 223 (2005)
28. Y. Li, M. Bowker, Surf. Sci. **285**, 219 (1993)
29. J.V. Barth, Surf. Sci. Rep. **40**, 75 (2000)
30. P.D. Cobden, C.A. de Wolf, M. Yu. Smirnov, A. Makeev, B.E. Nieuwenhuys, J. Mol. Catal. A **158**, 115 (2000)
31. M. Mundschau, B. Rausenberger, Platinum Metals Rev. **35**, 188 (1991)
32. P. Leerkamp, R.M. Wolf, B.E. Nieuwenhuys, J. Phys. Supplement, C6-227 (1988)
33. C. Voss, N. Kruse, Appl. Surf. Sci. **87/88**, 127 (1994)
34. C. Voss, N. Kruse, Appl. Surf. Sci. **94/95**, 186 (1995)
35. T. Visart de Bocarmé, N. Kruse, Chaos **12**, 1 (2002)
36. T.D. Chau, T. Visart de Bocarmé, N. Kruse, Surf. Interface Anal. **36**, 528 (2004)
37. J.W. Evans, J. Chem. Phys. **97**, 572 (1992)
38. Y. De Decker, G.A. Tsekouras, A. Provata, Th. Erneux, G. Nicolis, Phys. Rev. E **69**, 036203 (2004)
39. D.-J. Liu, X. Guo, J.W. Evans, Phys. Rev. Lett. **98**, 050601 (2007)
40. X. Guo, J.W. Evans, D.-J. Liu, Physica A **387**, 177 (2008)
41. C. Sachs, M. Hildebrand, S. Volkening, J. Wintterlin, G. Ertl, J. Chem. Phys. **116**, 5759 (2002)
42. X. Gao, Y. De Decker, J.W. Evans, Phys. Rev. E **82**, 021121 (2010), and references therein
43. S.R. de Groot, P. Mazur, *Non-Equilibrium Thermodynamics* (Dover Publications New York, 1984)
44. D. Fanelli, A.J. McKane, Phys. Rev. E **82**, 021113 (2010)
45. A.J. McKane, T.J. Newman, Phys. Rev. E **70**, 041902 (2004)